Journal of
Manufacturing and Materials Processing

MDPI

Article

Cooling Rate Modeling and Evaluation during Centrifugal Atomization Process

Sasha A. Cegarra [1,*], Jordi Pijuan [1] and María D. Riera [2]

[1] Eurecat, Centre Tecnològic de Catalunya, Unit of Metallic and Ceramic Materials, Plaça de la Ciència 2, 08243 Manresa, Spain; jordi.pijuan@eurecat.org
[2] Department of Mining, Industrial and ICT Engineering, Universitat Politècnica de Catalunya, Av. de les Bases de Manresa, 61-73, 08242 Manresa, Spain; md.riera@upc.edu
* Correspondence: sasha.cegarra@eurecat.org; Tel.: +34-938777373

Abstract: Centrifugal atomization is a rapid solidification technique involving fast cooling rates to produce high-quality powders. The final microstructure of the atomized particles is closely linked with the thermal history and cooling rates experienced during the atomization process. However, there is insufficient research on the temperature evolution of metal particles produced by this technique, and most works evaluate the thermal history of the droplet through semi-empirical correlations that lie outside the conditions where they were derived. In this work, the cooling rate of centrifugally atomized Al-4%Cu was studied via mathematical modelling and experimental validation. A heat transfer model was implemented, and the value of the convective heat transfer coefficient was obtained from the Whitaker semi-empirical correlation considering three cases of study for the thermophysical properties of the gas. The validity of the Whitaker correlation was experimentally evaluated by means of cooling rates based on the Secondary Dendrite Arm Spacing (SDAS) technique. The Whitaker correlation with the Reynolds and Prandtl numbers evaluated at the ambient temperature and the gas conductivity evaluated at the film temperature gave the best agreement with the experimental results, with cooling rates in the order of 10^5 Ks^{-1} for <32.5 μm powders atomized in He atmosphere.

Keywords: centrifugal atomization; cooling rate; secondary dendrite arm spacing

Citation: Cegarra, S.A.; Pijuan, J.; Riera, M.D. Cooling Rate Modeling and Evaluation during Centrifugal Atomization Process. *J. Manuf. Mater. Process.* **2023**, *7*, 112. https://doi.org/10.3390/jmmp7030112

Academic Editor: Steven Y. Liang

Received: 13 April 2023
Revised: 2 June 2023
Accepted: 6 June 2023
Published: 7 June 2023

1. Introduction

Centrifugal atomization is a rapid solidification technique that has been widely used for the production of metal powder for decades [1–3]. During this process, a molten metal stream falls onto a rotating disk, forming a liquid film on its surface. At the edge of the spinning disk, the centrifugal force exceeds the surface tension of the liquid, causing the melt to break up into droplets that solidify in flight in the form of powder. This technique finds wide application in metal powder production for several industrial processes, such as additive manufacturing [4,5], sintering processing [6–8], and thermal spray processes [9,10].

The centrifugal atomization technique offers many advantages, compared to more conventional gas and water atomization technologies, in terms of spherical shape, narrow particle size distribution, low satellite content, and high energy efficiency [11]. Although these characteristics are of greatest interest in many of the classic applications of metal powder, the need for new materials with a unique combination of properties is increasingly emerging to satisfy the powder metallurgy industry needs, which makes way to amplify the research spectrum in the use of this technology.

Some of these materials are rapidly solidified alloys, such as amorphous materials, which require strict control of the microstructure of the powder [12]. In the case of centrifugal atomization, the final microstructure of a powder is highly dependent on the thermal transport between a droplet in flight and a surrounding cooling gas once the droplet is ejected from the disk. During metal atomization, temperature differences of 1000 K or more

can be found between the molten droplet and the ambient gas. Therefore, the thermophysical properties of the gas vary considerably, and depending on the reference temperature, uneven results could be obtained. To address this limitation, several approaches have been used to account for the variation of gas properties that occur across the boundary layers in different processes, such as impulse atomization and gas atomization [13,14].

Most of the published works on the centrifugal atomization technique have been principally concerned with the design of a centrifugal atomizer, modes of liquid disintegration from a rotating disk, and the effect of process conditions on the particle size of the atomized powders [15–19], with the aim of contributing to the design and optimization of centrifugal atomizers in order to improve the stability of the process. However, although the thermal transport between a droplet and a surrounding gas has been extensively studied for processes such as gas atomization [20–24], plasma spray [25] and impulse atomization [13,26], very little information could be found in the literature for the centrifugal atomization process [27,28].

In the present work, a mathematical model has been carried out to describe the thermal behavior of Al-4%Cu centrifugally atomized particles that allows a better understanding of the heat transfer phenomena for this process. These calculations are based on the semi-empirical transfer laws [13,29], accounting for the temperature-dependent thermophysical properties of the gas evaluated at different conditions. The aim is to investigate the validity range of this semi-empirical correlation which predicts the cooling rate in molten metal centrifugal atomization. The results are compared with experimental cooling rate results obtained from Secondary Dendrite Arm Spacing (SDAS).

2. Mathematical Model

The heat transfer between a particle and the surrounding medium can be represented by Newton's cooling law, expressed by the following equation:

$$Q_c = A_s h_g (T_d - T_A) \tag{1}$$

where Q_c is the heat flow, A_s is the total surface area of a sphere particle, T_d is the temperature of the droplet, T_A is the ambient gas temperature inside the atomizer, and h_g is the total transfer coefficient. The application of this expression to a particular fluid–particle system has the obvious difficulty of knowing the value of h_g, a coefficient that incorporates the effect of convection, conduction, and radiation heat transfer mechanisms.

The high cooling rates experienced by a particle during the centrifugal atomization process [30], together with the high thermal conductivity of the metallic material, favors the homogeneous temperature distribution inside the droplet so that conduction is usually assumed negligible. This requires that the Biot number (Bi) be less than 0.1, where $Bi = hd/k_p$, h is the heat transfer coefficient to the gas, d is the diameter of the particle, and k_p is the thermal conductivity of the particle [31,32].

On the other hand, it has been shown that in low melting temperature metallic materials, the radiation heat transfer mechanism is negligible [33]. However, in this work, to account for precise results, the radiation contribution was taken into account. In this sense, the transfer of heat by radiation Q_r is expressed as follows:

$$Q_r = A_s S_t \varepsilon \left(T_d^4 - T_w^4 \right) \tag{2}$$

where S_t is the Stefan–Boltzmann constant, ε is the emissivity, and T_w is the wall temperature. A maximum value of emissivity ($\varepsilon = 1$) was considered for this work.

The variable hg from Equation (1) is a convective coefficient that can be quantified through the Nusselt number, Nu, which thermally characterizes the boundary layer between a particle of diameter d_p and a cooling gas by the following general semi-empirical equation [34]:

$$Nu = h_c \frac{d_p}{k_g} = a + cRe^m Pr^n \tag{3}$$

where h_c is the convective component of the heat transfer coefficient, and k_g is the thermal conductivity of the gas. The coefficients a and c, as well as the exponents m and n, are inherent to each system and must be determined experimentally.

The Reynolds numbers of the particle, Re, and Prandtl number of the gas, Pr, are given by the following equations:

$$Re = \frac{\rho_g (V_g - V_p) d_p}{\mu_g} \tag{4}$$

$$Pr = \frac{\mu_g C_{pg}}{k_g} \tag{5}$$

where ρ_g is the density of the cooling gas, V_p and V_g are the particle and gas velocity, respectively, μ_g is the dynamic viscosity, k_g is the thermal conductivity, and C_{pg} is the specific heat capacity of the gas.

Several approximations of the Nusselt number have been published [25,29,35–37], although the most frequently used in the field of metal atomization are the Ranz and Marshall [25] and the Whitaker [29] correlations, both defined for systems with a stationary particle interaction and a moving fluid.

The convective component of heat transfer coefficient h_c, described by the Ranz and Marshall correlation, is represented in the following equation:

$$Nu = h_c \frac{d_p}{k_g} = 2.0 + 0.6 Re^{1/2} Pr^{1/3} \tag{6}$$

Ranz and Marshall proposed the following values, a = 2, c = 0.6, m = 0.5, and n = 0.33, and they are valid for Reynolds between 0 and 200 and for Prandtl numbers between 0.68 and 0.72, with the gas properties evaluated at the average ambient temperature.

The convective component of heat transfer coefficient h_c, described by the Whitaker correlation, is represented in the following equation:

$$Nu = h_c \frac{d_p}{k_g} = 2.0 + \left(0.4 Re^{1/2} + 0.06 Re^{2/3}\right) Pr^{0.4} \left(\frac{\mu_A}{\mu_s}\right)^{1/4} \tag{7}$$

where μ_A/μ_s is the relationship between the viscosity at the ambient temperature μ_A and at the surface of the droplet μ_s. This approximation is valid for Nusselt number values between 3.5×10^4 and 7.6×10^4, Reynolds number between 0.71 and 380, and Prandtl numbers between 1 and 3.2 [13].

Both approximations, Ranz and Marshall and Whitaker, share the same equation structure. The fundamental difference between both approaches is the inclusion of the viscosity ratio in Whitaker's correlation. In their test conditions, where a stationary copper sphere was exposed to a stream of water, they found that water exhibited a significant change in viscosity with temperature. In addition, Whitaker's correlation separates the term relative to the Reynolds number into two contributions corresponding to the two types of regimes that are established in the laminar and wake regions found in the particle and fluid interaction.

A limitation of the former correlations, highlighted by numerous published works [14,21,31,38], is the validity of their extrapolation to systems that incorporate high temperatures, such as metal atomization techniques. In this sense, the work of Wiskel et al. [13] deserves to be highlighted. They proposed a modification of Whitaker's correlation applicable to the impulse atomization conditions for the production of Al-4.5%Cu powder, considering the temperature variation of the thermophysical properties of the gas through the boundary layer in high-temperature systems, expressed by the following relationship:

$$Nu = \frac{2B}{K_s(m+1)} \frac{T_s^{m+1} - T_A^{m+1}}{T_s - T_A} + \left(0.4 T_s^{\frac{1}{2}} + 0.06 Re_s^{\frac{2}{3}}\right) Pr_s \left(\frac{\mu_A}{\mu_s}\right)^{\frac{1}{4}} \tag{8}$$

where B is the pre-power coefficient from the variation of gas conductivity with temperature and is equal to 3.44×10^{-4}.

Overall, the evaluation of the thermophysical properties of the gas varies from author to author and must be addressed for each specific system through adjustments with experimental results. During centrifugal atomization, the initial droplet speed when the particles are ejected from the disk, and their trajectory during flight are the key parameters in the heat transfer mechanism. Zhao et al. studied the flow development and the velocity of the droplet depending on the melt flow rate in different conditions of atomization, in the case of a full spreading melt and the case of discontinuous melt flow rate on the atomization disc [39,40].

Zhao et al. [39] showed that for rotating disk velocities between 3000 to 60,000 rpm, specifically from the centrifugal atomization process studied in this work, the tangential component velocity of the atomizing disk is far superior to the radial component. Therefore, the tangential velocity of the atomizing disk can be used as an accurate estimate of the initial metal droplet velocity, to be 94.2 ms^{-1} at a rotating speed of 40,000 rpm.

After leaving the disk, the trajectory of the particles depends on the forces acting during their flight in the atomization chamber: buoyancy, gravity, and drag forces. Under the conditions of centrifugal atomization, the buoyancy effect is negligible, and it is not considered in this study [32].

After the particle is released from the disc, its movement is described into a plane tangent to the disc. In the vertical direction, gravity force is present, while the components of drag force appear in the horizontal and vertical directions. The drag coefficient is computed according to Yule et al. which considers a drag coefficient for particles in the micron range.

$$C_d = 18.5/Re^{0.6} \tag{9}$$

The acceleration components of the droplet are expressed as:

$$d^2x/dt^2 = -\rho_g(dx/dt)^2 A_s C_d/2m_d \tag{10}$$

$$d^2y/dt^2 = g - \rho_g(dy/dt)^2 A_s C_d/2m_d \tag{11}$$

where A_s and m_d is the area of the mass of the droplet, respectively.

The density and viscosity of the gas in which the particle moves and cools, as well as its size and speed with respect to that of the gas, determine the drag force to which it is subjected and the type of fluid dynamic regime that develops. In addition, in its flight inside the atomizer chamber, the particle, initially driven by the centrifugal force imposed by the rotating disk, loses speed until it collides with the wall of the chamber or drops to its bottom. The progressive change in temperature and, therefore, in the thermal gradient between the particle and the gas, as well as the decrease in the speed, continuously modify the heat transfer conditions. Hence, it is important to address the dependent thermophysical properties of the gas to accurately calculate the heat transfer and cooling rate in the process of droplet solidification during centrifugal atomization.

In this work, the Whitaker correlation [29] and the Whitaker modified correlation [13], which considers the effect of gas viscosity, were used to determine the Nu number. The thermal gas conductivity k_g in Equations (6) and (7) was evaluated at three different temperatures: Case 1, at gas ambient temperature T_A; Case 2, at film temperature T_f, which is the median temperature between the droplet and ambient gas temperatures, $T_f = (T_d + T_A)/2$; and Case 3, at droplet surface temperature T_d.

2.1. Cooling Rate Calculation

The size of the solidification microstructure is related to the solidification cooling over the entire local solidification process [11]. Therefore, the cooling rate is computed as the

difference between liquidus and solidus temperature with respect to the local solidification time:

$$CR = (T_l - T_s)/t_{ls} \quad (12)$$

where T_l and T_s are the liquidus and solidus temperature, and t_{ls} is the time required for each full solidification state.

During the solidification period, an equivalent heat capacity coefficient is computed to consider solidification enthalpy [41].

$$C_{p,app} = \Delta H_m/(T_l - T_s) + C_{p,s} + C_{p,l}/2 \quad (13)$$

where ΔH_m is the latent heat of fusion, $C_{p,l}$ is the specific heat capacity of the material in a liquid state, while $C_{p,s}$ is the specific heat capacity of the material in a solid state, and T_l and T_s are the liquidus and solidus temperatures.

2.2. Properties of Atomization Gas and Alloys

Trajectories and thermal history of particles of different sizes (32.5, 60, 90.5, 115.5, 137.5 and 165 µm) were computed to correspond with the median particle size on each particle size range analyzed in this work. Two gas atmospheres (He and Ar at 25 °C and 1 atm) and two initial melt superheat temperatures (250 K and 400 K) were considered. The initial velocity of droplets was computed according to the tangential velocity in an atomization disc of 45 mm diameter spinning at 40,000 rpm. Values of thermophysical properties of Al-4%Cu alloy are shown in Table 1 [42].

Table 1. Physical and thermal properties of alloy Al-4%Cu.

Parameter	Symbol (Unit)	Value
Liquidus Temperature	T_l (K)	921
Solidus Temperature	T_s (K)	845
Density of the droplet	ρ_d (kg m^{-3})	2540
Specific Heat of Liquid Alloy	$C_{p,l}$ (J kg^{-1} K^{-1})	910
Specific Heat of Solid Alloy	$C_{p,s}$ (J kg^{-1} K^{-1})	1178
Latent Heat of Fusion	ΔH_f (J kg^{-1})	381,774

An exponential equation is used to define He and Ar thermal conductivity, dynamic viscosity, and density depending on temperature [21]. Gas-specific heat capacity is assumed to be constant. The thermophysical properties of gases are shown in Table 2 [21].

Table 2. Thermophysical properties of He and Ar.

Parameter	Ar	He
Density ρ_g (kg/m^3)	$486.61/T$	$48.774/T$
Dynamic Viscosity μ_g (Pa·s)	$3.7763{\cdot}10^{-7}{\cdot}T^{0.71832}$	$4.3679{\cdot}10^{-7}{\cdot}T^{0.67016}$
Thermal Conductivity k_g (W m^{-1}K^{-1})	$2.5943{\cdot}10^{-4}{\cdot}T^{0.74021}$	$2.1588{\cdot}10^{-3}{\cdot}T^{0.74210}$
Specific Heat Capacity C_{pg} (J kg^{-1} K^{-1})	520.8	5197

3. Materials and Methods

3.1. Materials

Commercial aluminum alloy Al 1050 and electrolytic copper with a purity of 99.9% were induction melted in a mass composition of Al-4%Cu prior to atomization. This alloy was used since many studies on the correlation between Secondary Dendrite Arm Spacing of Al-4%Cu alloys and cooling rate are found in the literature [43–46].

3.2. Atomization

A schematic diagram of the centrifugal atomizer pilot plant is shown in Figure 1. The stainless steel atomization chamber measures 2.5 m in diameter and 4 m in height. The

melting system consists of a crucible, an alumina stopper rod, and a thermocouple as a temperature controller. The crucible with a 3.5 mm hole was made of alumina, and the metal was heated via induction. A stopper rod was fitted to the hole to control the molten metal exit. A 45 mm H13 steel spinning disk with a ZrO_2 coating was used for atomizing the molten metal. A water-cooling system for the disk was used to guarantee the integrity of the disk due to the high temperatures of atomization. The atmosphere controlling unit consists of a vacuum pump with levels down to 1 Pa and an inert gas supply.

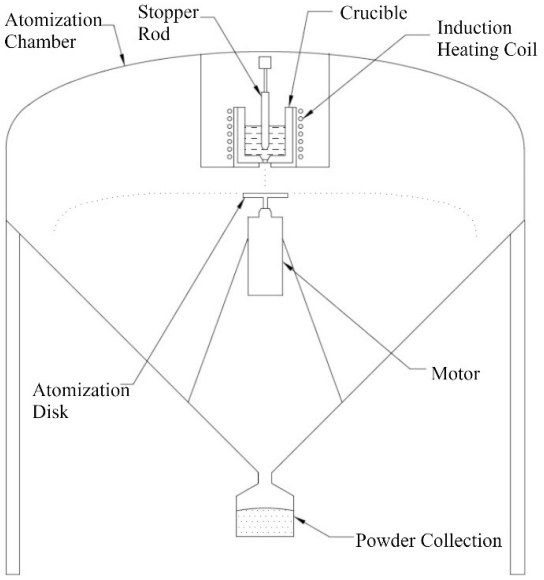

Figure 1. Schematic diagram of the centrifugal atomization pilot plant.

Prior to melting and atomization, the vacuum pump was run to ensure low oxygen content, being backfilled with up to 1 atm of He or Ar according to the atomization. The raw materials were induction melted to temperatures of 850 K and 1050 K, which corresponds to a superheating temperature of 250 K and 400 K, respectively. To ensure maximum homogenization of all elements, the molten metal atomization temperature was kept constant for 10 min. Molten metal was poured gravity onto the atomization disc rotating at 40,000 rpm. Figure 2 shows observations on the melt performance on the rotating disk during atomization made with a Vision Research Phantom v311 Monochrome high-speed camera.

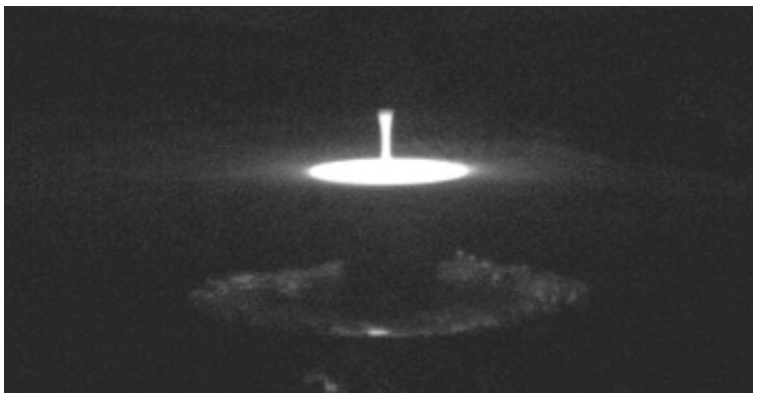

Figure 2. Centrifugal atomization process in operation.

A series of atomization runs were carried out with the variation of the inert gas atmosphere and the alloy melt superheat temperature as the main parameters of the atomization process. The experimental process parameters of atomization are shown in

Table 3. A total of 350 g of materials were melted and atomized for each experiment, where only one parameter was changed, leaving the others fixed. The mass median particle size and the log-normal standard deviation (σ) were calculated.

Table 3. Experimental processing parameters of atomization.

Run #	Gas Type	Superheat Melt Temperature	D_{50} (μm)	σ
1	100% Ar	400	113	1.82
2	100% He	400	119	1.63
3	100% Ar	250	107	1.64
4	100% He	250	104	1.69

3.3. Powder Characterization

Following atomization, each of the as-produced powders was collected and sieved according to ASTM-B214-07 for 15 min with a Filtra FTL-0150 electromagnetic digital sieving machine into six fractions: 25–45 μm, 75–45 μm, 106–75 μm, 125–106 μm, 150–125 μm, and 180–150 μm. Samples of each size fraction from each experiment were subsequently metallographically prepared. A total of 25 samples were cold mounted using epoxy resin, mixing the metal powder with a small amount of epoxy resin and pouring it into the bottom of the specimen cup. Samples were ground using wet grit SiC paper of 600-800-1200-2400-4000, respectively, for one minute at a force of 20 N. The specimens were polished with diamond suspension solution of 6 μm, 3 μm, and 1 μm for 10 min in each step, applying a force of 20 N, and finally finishing with colloidal dispersions of silica (SiO_2) for 10 min. The procedures were applied according to ASTM-B215, using standard metallographic methods for uncompacted metal powders [47]. The shape, microstructure and SDAS of the powders were investigated by using an Ultra Plus Field Emission Scanning Electron Microscope (SEM).

3.4. Secondary Dendrite Arm Spacing Measuring Method

SEM images were used to measure SDAS with the image analysis software Olympus Stream Version 2.4.4, with enabled direct length readings. A minimum of 10 particles were analyzed for each size range, and at least 10 dendrites were measured in each particle. The secondary dendrites were evaluated according to the following equation:

$$SDAS = 2/N_{arms} - 1 \quad (14)$$

where N represents the number of secondary arms counted along one side of the primary arm, and L is measured as the length parallel to the primary arm between the first and the last secondary dendrite arm, as shown in Figure 3.

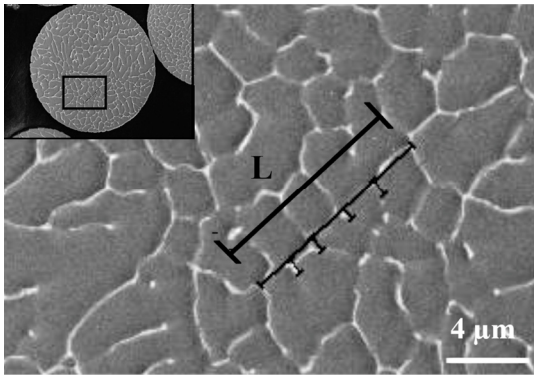

Figure 3. Schematic representation of SDAS measurement.

4. Results and Discussion

4.1. Metallographic Analysis

SEM micrographs from Figure 4 show the solidification structure for Al-4%Cu droplets in the 75–45 µm size range observed in each experiment. The microstructure of the atomized Al-4%Cu powders consisted of a fine equiaxed dendrite structure which is typical for all-size droplets atomized in this study. From these micrographs, no visible changes are shown in the effect of melting superheat temperature on the resulting microstructure. However, the gas composition does have a significant effect on the microstructure, resulting in fine-scale microstructure for powders atomized in He, as opposed to those atomized in Ar.

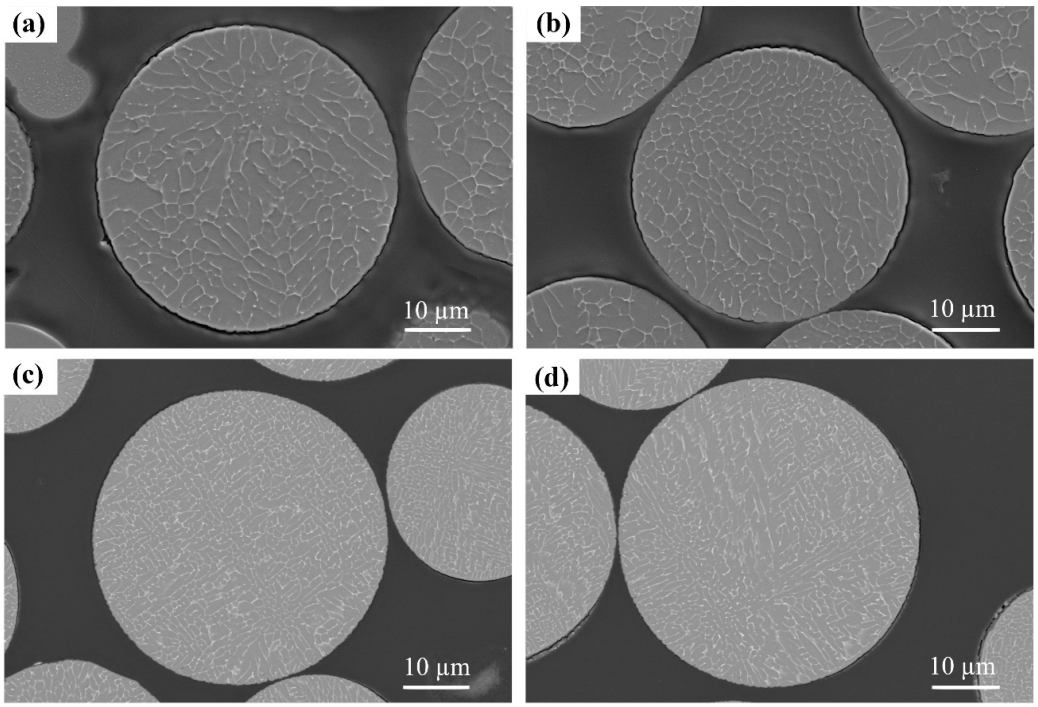

Figure 4. Micrographs of Al-4%Cu centrifugal atomized particles (size fraction from 45 to 75 µm) at different gas compositions and melt superheat temperatures: (**a**) Ar-400 K; (**b**) Ar-250 K; (**c**) He-400 K; and (**d**) He-250 K.

4.2. Secondary Dendrite Arm Spacing—Cooling Rate Correlation

The relationship between secondary arm spacing λ and cooling rate R is obtained by means of a correlation analysis leading to the following empirical logarithmic equation [48,49]:

$$\lambda = \lambda_0 R^{-n} \tag{15}$$

where R is the cooling rate and n and λ_0 are constants derived empirically where the SDAS is compared to the cooling rate. In this work, Mullis' correlation [45], based on several published experiments for Al-Cu alloy, was used to convert the SDAS results to cooling rate as a function of the mean particle size.

$$\lambda = 58.7R^{-0.355} \tag{16}$$

The relationship between SDAS with respect to the corresponding fraction size for each atomization run is plotted in Figure 5a, whilst a direct comparison of the SDAS to cooling rate as a function of the mean particle size is shown in Figure 5b [46].

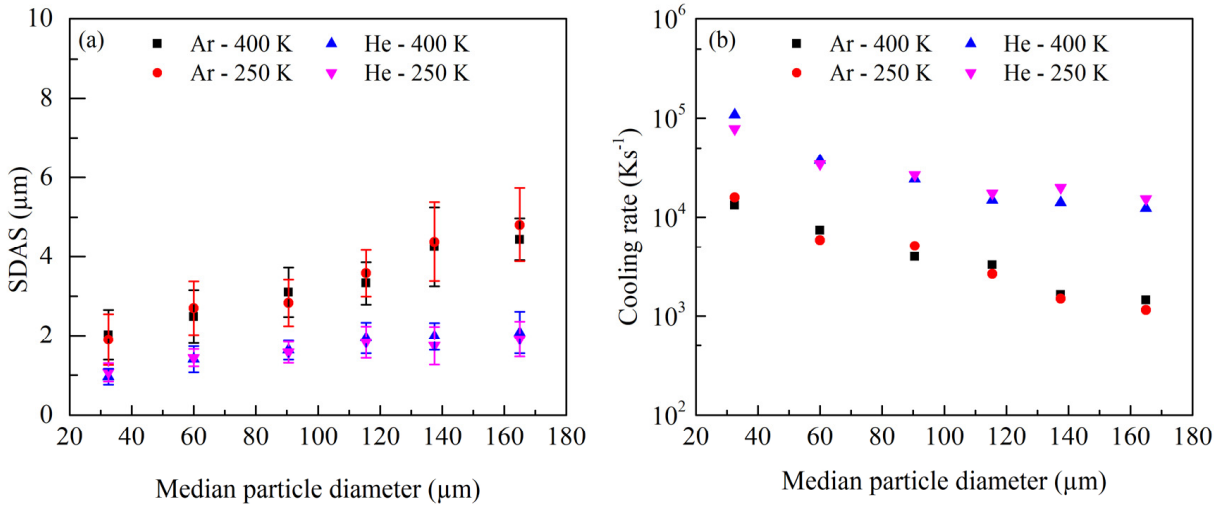

Figure 5. (**a**) Experimental results of the SDAS as a function of the mean particle size for a corresponding size range; (**b**) calculated cooling rate as a function of the mean particle size for a corresponding size range.

Error bars in Figure 5a represent the standard deviation calculated from the data of corresponding fraction size. This standard variation is caused by the cumulative effect of measurement errors inherent to the SDAS measurement method, the thermal history of each particle resulting in different microstructures, and the range of particle sizes experiencing different cooling rates.

The results capture a refinement in dendritic structure with decreasing particle size. The length of SDAS ranges from 2 to 5 μm for particles atomized in the Ar atmosphere. However, for particles atomized in the He atmosphere, the length of SDAS ranges from 1 to 2 μm. As expected, SDAS, for a given particle size, is finer for atomization in He relative to Ar due to the high thermal conductivity of He, whereas the melt superheat temperature does not seem to affect the microstructure. Based on these values, cooling rates range from 10^3 to 10^4 Ks^{-1} for particles atomized in the Ar atmosphere to 10^4 to 10^5 Ks^{-1} for particles atomized in the He atmosphere. These values are in agreement with those previously reported by Östürk [27], although the processing parameters in their study differ from this work.

4.3. Theoretical Cooling Rate

Figure 6 shows the theoretically cooling rate as a function of mean particle diameter for the three cases of study considered in this work for the evaluation of the Nusselt number *Nu*:

- Case 1: Whitaker correlation with k_g, *Re* and *Pr* evaluated at the ambient temperature T_A;
- Case 2: Whitaker correlation with k_g evaluated at the film temperature $T_f = (T_d + T_A)/2$ and *Re* and *Pr* evaluated at the ambient temperature T_A;
- Case 3, Wiskel modified correlation with k_g evaluated at the droplet surface temperature T_d and *Re* and *Pr* evaluated at the ambient temperature T_A.

The cooling rate notably changes with the different conditions studied in this work. Both the thermophysical properties of the He and the Ar atmosphere vary considerably from the droplet surface temperature T_d to the ambient temperature T_A, confirming that these differences can have a significant impact on the centrifugal atomization heat transfer evaluation.

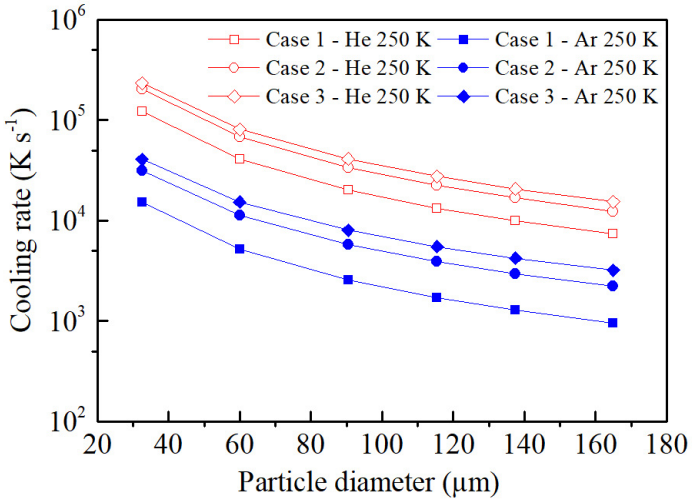

Figure 6. Theoretically calculated cooling rate as a function of the mean particle diameter for particles atomized in Ar and He atmospheres at 250 K superheat temperature. Gas properties were evaluated at three different temperatures: case 1, at gas ambient temperature T_A; case 2, at film temperature T_f; case 3, at droplet surface temperature T_d.

The curves for Case 1 have the lowest values of cooling rate, between 2.7×10^3 Ks^{-1} and 3×10^4 Ks^{-1} for particles atomized in the Ar atmosphere and between 1.7×10^4 Ks^{-1} and 2×10^5 Ks^{-1} for particles atomized in the He atmosphere. The thermal conductivity k_g evaluated at the ambient temperature T_A corresponds to systems where the temperature differences between the particle and the fluid are small. Therefore, the thermophysical properties of the gas in the boundary layer do not vary significantly. Despite this and the great temperatures differences found in metallurgical processes such as centrifugal atomization, the evaluation of these properties continues to be evaluated at the ambient temperature for a large number of processes [20,50,51], which may introduce errors in the final cooling rate results.

Regarding Case 2, although it has been suggested to use the Whitaker correlation with the evaluation of k_g at the ambient temperature [24], using these values at the film temperature T_f is, a priori, a reasonable approximation for systems where the temperature differences in the boundary layer may become larger than in Case 1. Figure 4 shows an increase in the cooling rate values in Case 2 compared to Case 1.

Finally, Case 3 corresponds to the case where the thermal conductivity k_g is measured at the droplet surface temperature T_d, that is, when the relative velocity between the atomized particle and the gas approaches zero. In this approach, the Wiskel correlation [13] was used to account for the temperature dependency of k_g in the boundary layer for systems where the temperature differences between the particle and the fluid are big (approx. 1000 K). Case 3 gives the highest values of cooling rate from the three cases of study.

As expected, as the temperature where the thermal conductivity k_g is measured increases, the cooling rate values also increase. It is evident that the cooling rate notably changes with the different conditions, following the same pattern either for particles atomized in Ar or He gas, stating the importance of determining at which temperature (ambient, film of surface temperature) to calculate the thermophysical properties of the gas.

4.4. Experimental Validation of the Model

Figure 7 shows the cooling rate calculated theoretically for the three cases of study, as well as the cooling rate calculated experimentally and through Mullis' empirical correlation for Al-4%Cu [45].

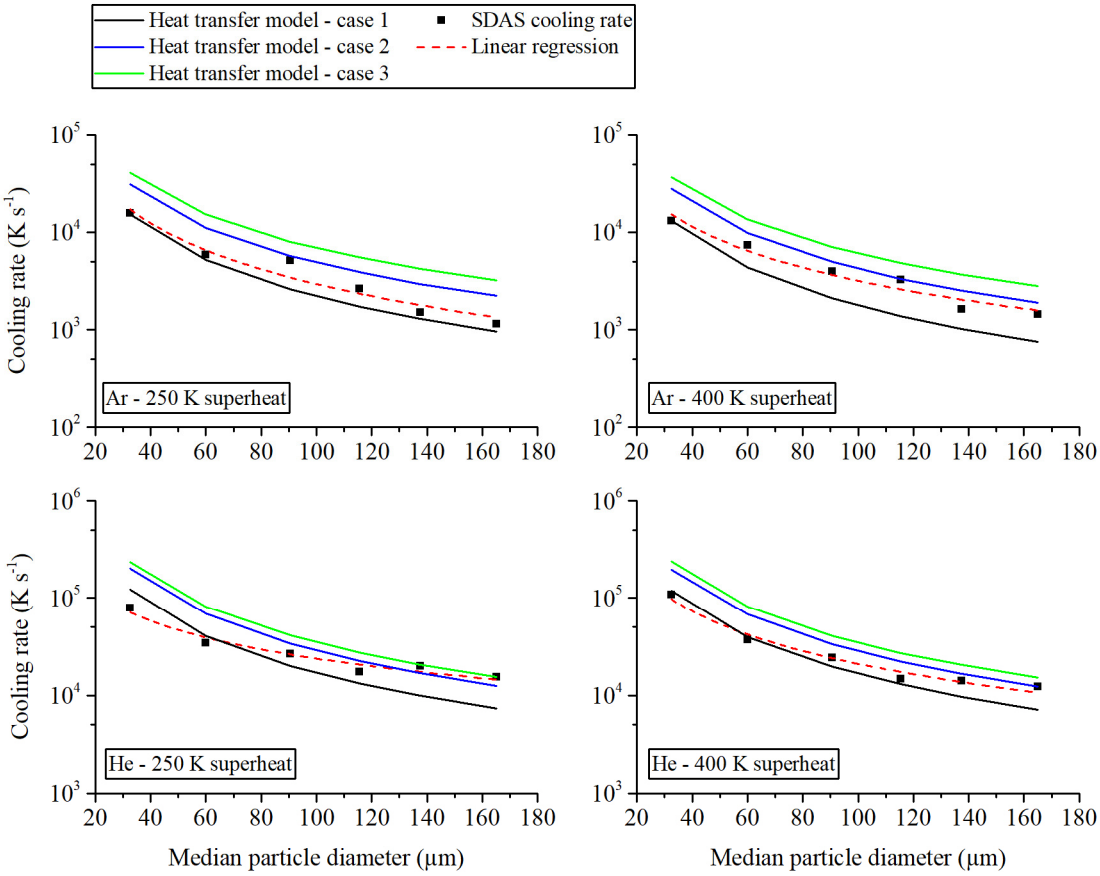

Figure 7. Comparison between the theoretically calculated cooling rate for the three cases of study and the calculated cooling rates based on SDAS measurements.

It becomes evident that in Case 3, where k_g is evaluated at the surface temperature of the droplet T_d, the model yields overestimated cooling rate values. It is worth mentioning that Wiskel reported that the gas properties evaluated at T_d fit better for the impulse atomization process [7]. This may be due to the low particle velocity achieved during impulse atomization. When the relative velocity between the gas and the particle approaches zero, it seems of a good agreement to evaluate the gas properties at the droplet surface temperature T_d. However, during the centrifugal atomization process, particles experience a high velocity provided by the disk speed. Thus, the surrounding gas renovation around the particle is faster than during impulse atomization; therefore, evaluating k_g at the surface temperature of the droplet does not correlate with the experimental results.

From the comparison between the theoretical cooling rate and the experimental cooling rate calculation, it is not clear whether the evaluation of k_g using the Whitaker correlation at the film temperature T_f gives better results than evaluating k_g at the ambient temperature T_A. For small particle sizes, evaluating the properties of the gas at the ambient temperature correlates better by comparing both results, theoretical and experimental approaches, while as the particle size increases, Case 2 gives better results. However, it is known that to calculate the convective heat transfer coefficient h_c, the use of k_g at ambient temperatures may introduce errors for higher temperatures systems. In this sense, the evaluation of the thermophysical properties of the gas for the centrifugal atomization process is recommended to be addressed using Whitaker's correlation, which considers the temperature differences through the ratio of the dynamic viscosities at the droplet surface temperature T_d and the ambient temperature T_A, with the evaluation of the thermal conductivity of the gas k_g from the Nusselt number at the film temperature T_f.

From the heat transfer model, it is evident that the cooling rate of particles depends largely on the alloy in terms of density, specific heat, and melting temperature. In addition,

in the case of the centrifugal atomization process, in particular, the cooling rate also depends on the size of the particle in trajectory, the initial velocity of the particle, and the properties of the gas. In this sense, by varying the properties of the gas for a specific alloy, and for a known initial velocity provided by the disk speed, the heat transfer process gives different results for the cooling rate of the particles.

The proposed approach does not consider the effect of radiation, which in cases of high melt temperature alloys, its contribution is significant. Additionally, for simplicity, the model considers just one particle solidifying at a time with no interaction with each other, which otherwise would contribute to a local temperature increase resulting in a lower cooling rate. Finally, the use of a Mullis semi-empirical relationship is applicable to Al-4%Cu alloys. Although these limitations arise, this work suggests further advances in terms of modelling the solidification process in the centrifugal atomization process.

4.5. Thermal Evolution of the Atomized Particles

Figure 8 shows the temperature profile for a 60 µm and 137 µm droplet atomized in the Ar and He atmosphere, with a melt superheat temperature of 250 K computed using Case 2 in the mathematical model. It can be seen that the temperature decreases rapidly with changing the gas composition from Ar to He. For a 60 µm particle atomized in an Ar atmosphere, it takes 8.7×10^{-3} s to completely solidify, whereas, for the same particle size atomized in a He atmosphere, it takes 1.6×10^{-3} s to solidify. Therefore, for the same particle size, solidification occurs earlier in a He atmosphere, meaning that the solidification of droplets occurs in a nearer position of the atomization disc than in an Ar atmosphere.

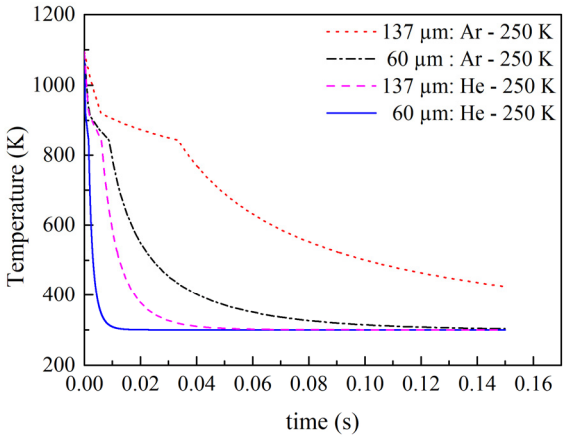

Figure 8. The temperature profile of centrifugally atomized particles for Case 2 of this study, for particles atomized in Ar and He atmospheres at 250 K superheat temperature.

Moreover, Figure 8 shows that droplet temperature decreases faster with decreasing powder size from 137 to 60 µm within the same gas composition. For example, particles of 60 µm atomized in He atmosphere take 3.7×10^{-4} s, while particles of 137 µm atomized in the same atmosphere take 6.07×10^{-3} s to completely solidify, increasing one order of magnitude. These results confirm that while the gas composition is effective in influencing the cooling rate of the atomized particles, the cooling rate has a strong dependence on droplet size.

5. Conclusions

A mathematical model was employed to describe the thermal behavior of Al-4%Cu centrifugally atomized particles coupled with the characterization of the powder by the Secondary Dendrite Arm Spacing method. This contribution discusses the effect of the temperature-dependent thermophysical properties of the gas evaluated at different conditions.

To calculate cooling rates to be consistent with those determined experimentally by the semi-empirical model proposed by Mullis correlation, the gas thermal conductivity k_g requires the evaluation of the thermal conductivity of the gas at the film temperature T_f, which accounts for the fast-surrounding gas renovation when the particle is expelled from the disk.

From the SDAS measurements, the cooling rate was calculated to be from 10^4 to 10^5 Ks^{-1} for particles atomized in a He atmosphere and from 10^3 to 10^4 Ks^{-1} for particles atomized in an Ar atmosphere, where He provides the highest rates of heat transfer compared to Ar due to its higher thermal conductivity.

The realization of the full potential of centrifugal atomization is limited by the lack of in-depth scientific understanding of the process. Therefore, and since the process of droplet solidification during flight is not available experimentally, this study offers new insights into the scientific knowledge in this field in order to improve the process in terms of the predictability of the resulting powder atomized by the centrifugal atomization process.

Author Contributions: Conceptualization, S.A.C. and J.P.; methodology, S.A.C. and J.P.; software, J.P.; validation, S.A.C. and J.P.; formal analysis, S.A.C. and J.P.; investigation, S.A.C., J.P. and M.D.R.; resources, S.A.C. and J.P.; data curation, S.A.C. and J.P.; writing—original draft preparation, S.A.C.; writing—review and editing, S.A.C., J.P. and M.D.R.; visualization, S.A.C. and J.P.; supervision, J.P. and M.D.R.; project administration, J.P.; funding acquisition, M.D.R. All authors have read and agreed to the published version of the manuscript.

Funding: This research was funded by the Agència de Gestió d'Ajuts Universitaris i de Recerca under grant number 2019 DI-19.

Data Availability Statement: Data are contained within the article.

Conflicts of Interest: The authors declare no conflict of interest.

References

1. Frost, A. Rotary Atomization in the Ligament Formation Mode. *J. Agric. Eng. Res.* **1981**, *26*, 63–78. [CrossRef]
2. Klaphaak, D. Method of Centrifugal Atomization. U.S. Patent 3,720,737, 13 March 1973.
3. Mandal, S.; Sadeghianjahromi, A.; Wang, C.C. Experimental and Numerical Investigations on Molten Metal Atomization Techniques—A Critical Review. *Adv. Powder Technol.* **2022**, *33*, 103809. [CrossRef]
4. Popov, V.V.; Grilli, M.L.; Koptyug, A.; Jaworska, L.; Katz-demyanetz, A.; Klobčar, D.; Balos, S.; Postolnyi, B.O.; Goel, S. Powder Bed Fusion Additive Manufacturing Using Critical Raw Materials: A Review. *Materials* **2021**, *14*, 909. [CrossRef]
5. Sames, W.J.; List, F.A.; Pannala, S.; Dehoff, R.R.; Babu, S.S. The Metallurgy and Processing Science of Metal. *Int. Mater. Rev.* **2016**, *61*, 315–360. [CrossRef]
6. Narasimhan, K.S.; Semel, F.J. Sintering of Powder Mixtures and the Growth of Ferrous Powder Metallurgy. *Mater. Chem. Phys.* **2001**, *67*, 56–65. [CrossRef]
7. Deirmina, F.; Pellizzari, M.; Federici, M. Production of a Powder Metallurgical Hot Work Tool Steel with Harmonic Structure by Mechanical Milling and Spark Plasma Sintering. *Metall. Mater. Trans. A* **2017**, *48*, 1910–1920. [CrossRef]
8. Kim, J.H.; Lee, J.W.; Kim, K.H.; Lee, C.B. Preliminary Study on the Fabrication of Particulate Fuel through Pressureless Sintering Process. *Sci. Technol. Nucl. Install.* **2016**, *2016*, 3717361. [CrossRef]
9. Henao, J.; Concustell, A.; Cano, I.G.; Dosta, S.; Cinca, N.; Guilemany, J.M.; Suhonen, T. Novel Al-Based Metallic Glass Coatings by Cold Gas Spray. *Mater. Des.* **2016**, *94*, 253–261. [CrossRef]
10. Bauckhage, K. Fundamentals of Melt Atomization, Spray Forming and Deposition. In Proceedings of the International Conference on Liquid Atomization and Spray Systems ICLASS, Sorrento, Italy, 13–17 July 2003.
11. Bogno, A.-A.; Henein, H.; Uhlenwinkel, V.; Gärtner, E. Single Fluid Atomization Fundamentals. In *Metal Sprays and Spray Deposition*; Henein, H., Uhlenwinkel, V., Fritsching, U., Eds.; Springer: Cham, Switzerland, 2017; pp. 9–46, ISBN 978-3-319-52687-4.
12. Pijuan, J.; Cegarra, S.A.; Dosta, S.; Albaladejo-Fuentes, V.; Riera, M.D. Centrifugal Atomization of Glass-Forming Alloy $Al_{86}Ni_8Y_{4.5}La_{1.5}$. *Materials* **2022**, *15*, 8159. [CrossRef]
13. Wiskel, J.B.; Henein, H.; Maire, E. Solidification Study of Aluminum Alloys Using Impulse Atomization: Part I: Heat Transfer Analysis of an Atomized Droplet. *Can. Metall. Q.* **2002**, *41*, 97–110. [CrossRef]
14. Poulikakos, D.; Waldvogel, J.M. Heat Transfer and Fluid Dynamics in the Process of Spray Deposition. *Adv. Heat Transf.* **1996**, *28*, 1–74. [CrossRef]
15. Zhang, L.P.; Zhao, Y.Y. Particle Size Distribution of Tin Powder Produced by Centrifugal Atomisation Using Rotating Cups. *Powder Technol.* **2017**, *318*, 62–67. [CrossRef]

16. Sungkhaphaitoon, P.; Plookphol, T.; Wisutmethangoon, S. Design and Development of a Centrifugal Atomizer for Producing Zinc Metal Powder. *Int. J. Appl. Phys. Math.* **2012**, *2*, 77–82. [CrossRef]
17. Sungkhaphaitoon, P.; Wisutmethangoon, S.; Plookphol, T. Influence of Process Parameters on Zinc Powder Produced by Centrifugal Atomisation. *Mater. Res.* **2017**, *20*, 718–724. [CrossRef]
18. Zhao, Y.Y.; Jacobs, M.H.; Dowson, A.L. Liquid Flow on a Rotating Disk Prior to Centrifugal Atomization and Spray Deposition. *Metall. Mater. Trans. B* **1998**, *29*, 1357–1369. [CrossRef]
19. Kumar, P.; Sarkar, S. Experimental Investigation of Liquid Disintegration on Slotted Disc in Centrifugal Atomization Process. *Chem. Eng. Res. Des.* **2019**, *145*, 76–84. [CrossRef]
20. Freyberg, A.V.; Henein, H.; Uhlenwinkel, V.; Buchholz, M. Droplet Solidification and Gas-Droplet Thermal Coupling in the Atomization of a Cu-6Sn Alloy. *Metall. Mater. Trans. B* **2003**, *34*, 243–253. [CrossRef]
21. Ciftci, N.; Ellendt, N.; Coulthard, G.; Soares Barreto, E.; Mädler, L.; Uhlenwinkel, V. Novel Cooling Rate Correlations in Molten Metal Gas Atomization. *Metall. Mater. Trans. B* **2019**, *50*, 666–677. [CrossRef]
22. Zheng, B.; Lin, Y.; Zhou, Y.; Lavernia, E.J. Gas Atomization of Amorphous Aluminum: Part I. Thermal Behavior Calculations. *Metall. Mater. Trans. B* **2009**, *40*, 768–778. [CrossRef]
23. He, S.; Liu, Y.; Guo, S. Cooling Rate Calculation of Non-Equilibrium Aluminum Alloy Powders Prepared by Gas Atomization. *Rare Met. Mater. Eng.* **2009**, *38*, 353–356.
24. Ellendt, N.; Lumanglas, A.M.; Moqadam, S.I.; Mädler, L. A Model for the Drag and Heat Transfer of Spheres in the Laminar Regime at High Temperature Differences. *Int. J. Therm. Sci.* **2018**, *133*, 98–105. [CrossRef]
25. Abderrahmane, A.; Mohamed, A.; Abdelkader, N.; El Ganaoui, M.; Pateyron, B. Ranz and Marshall Correlations Limits on Heat Flow Between a Sphere and Its Surrounding Gas at High Temperature. *Therm. Sci.* **2015**, *19*, 1521–1528. [CrossRef]
26. Ellendt, N.; Schmidt, R.; Knabe, J.; Henein, H.; Uhlenwinkel, V. Spray Deposition Using Impulse Atomization Technique. *Mater. Sci. Eng. A* **2004**, *383*, 107–113. [CrossRef]
27. Öztürk, S.; Arslan, F.; Öztürk, B. Effect of Production Parameters on Cooling Rates of AA2014 Alloy Powders Produced by Water Jet Cooled, Rotating Disc Atomisation. *Powder Metall.* **2003**, *46*, 342–348. [CrossRef]
28. Zhu, X.; Ding, B.; Wang, H.; He, X.Y.; Tan, Y.; Liao, Q. Numerical Study on Solidification Behaviors of a Molten Slag Droplet in the Centrifugal Granulation and Heat Recovery System. *Appl. Therm. Eng.* **2018**, *130*, 1033–1043. [CrossRef]
29. Whitaker, S. Forced Convection Heat Transfer Correlations for Flow in Pipes, Past Flat Plates, Single Cylinders, Single Spheres, and for Flow in Packed Beds and Tube Bundles. *AIChE J.* **1972**, *18*, 361–371. [CrossRef]
30. Cegarra Salges, S.A.; Pijuan, J.; Hernández, R.; Riera, M.D. Effect of Processing Parameters on Copper Powder Produced by Novel Hybrid Atomisation Technique. *Powder Metall.* **2020**, *63*, 142–148. [CrossRef]
31. Meharabian, R.; Hsu, S.C.; Levi, C.G.; Kou, S. Heat Flow Limitations in Rapid Solidification Processing. In *Advances in Metal Processing*; Burke, J.J., Meharabian, R., Weiss, V., Eds.; Plenum Press: New York, NY, USA, 1981; pp. 13–44, ISBN 9781461583028.
32. Yule, A.J.; Dunkley, J.J. *Atomization of Melts*, 1st ed.; Oxford University Press: Oxford, UK, 1994; ISBN 0198562586.
33. Gianoglio, D.; Ciftci, N.; Armstrong, S.; Uhlenwinkel, V.; Battezzati, L. On the Cooling Rate-Microstructure Relationship in Molten Metal Gas Atomization. *Metall. Mater. Trans. A* **2021**, *52*, 3750–3758. [CrossRef]
34. Ranz, W.E.; Marshal, W.R. Evaporation from drops. *Chem. Eng. Prog.* **1952**, *48*, 141–146.
35. Lewis, J.A.; Gauvin, W.H. Motion of Particles Entrained in a Plasma Jet. *AIChE J.* **1973**, *19*, 982–990. [CrossRef]
36. Young, R.M.; Pfender, E. Nusselt Number Correlations for Heat Transfer to Small Spheres in Thermal Plasma Flows. *Plasma Chem. Plasma Process.* **1987**, *7*, 211–229. [CrossRef]
37. Haghighatjoo, M. A Numerical Investigation of Free-Fall Swirling Gas Atomization Process. Masters's Thesis, Concordia University, Montreal, QC, Canada, November 2020.
38. Lee, E.S.; Ahn, S. Solidification Progress and Heat Transfer Analysis of Gas-Atomized Alloy Droplets during Spray Forming. *Acta Metall. Mater.* **1994**, *42*, 3231–3243. [CrossRef]
39. Zhao, Y.Y. Analysis of Flow Development in Centrifugal Atomization: Part I. Film Thickness of a Fully Spreading Melt. *Model. Simul. Mater. Sci. Eng.* **2004**, *12*, 959–971. [CrossRef]
40. Zhao, Y.Y. Analysis of Flow Development in Centrifugal Atomization: Part II. Disintegration of a Non-Fully Spreading Melt. *Model. Simul. Mater. Sci. Eng.* **2004**, *12*, 973–983. [CrossRef]
41. Produktionstechnik, D.F.; Ciftci, N. Cooling Strategies for the Atomization of Glass-Forming Alloys. Ph.D. Thesis, University of Bremen, Bremen, Germany, 2020.
42. Çengel, Y.A. *Heat Transfer: A Practical Approach*, 1st ed.; McGraw-Hill: New York, NY, USA, 1998.
43. Anyalebechi, P.N. Effects of Alloying Elements and Solidification Conditions on Secondary Dendrite Arm Spacing in Aluminum Alloys. In Proceedings of the TMS Annual Meeting, Charlotte, NC, USA, 14–18 March 2004; Volume 2004, pp. 217–233.
44. Wiskel, J.B.; Navel, K.; Henein, H.; Maire, E. Solidification Study of Aluminum Alloys Using Impulse Atomization: Part II. Effect of Cooling Rate on Microstructure. *Can. Metall. Q.* **2002**, *41*, 193–204. [CrossRef]
45. Mullis, A.M.; Farrell, L.; Cochrane, R.F.; Adkins, N.J. Estimation of Cooling Rates during Close-Coupled Gas Atomization Using Secondary Dendrite Arm Spacing Measurement. *Metall. Mater. Trans. B* **2013**, *44*, 992–999. [CrossRef]
46. He, C.; Yu, W.; Li, Y.; Wang, Z.; Wu, D.; Xu, G. Relationship between Cooling Rate, Microstructure Evolution, and Performance Improvement of an Al-Cu Alloy Prepared Using Different Methods. *Mater. Res. Express* **2020**, *7*, 116501. [CrossRef]

47. Leander, F.; Pease, D.L. Metallography and Microstructures of Powder Metallurgy Alloys. In *Metallography and Microstructures Handbook*; Voort, V., Baldwin, W., Eds.; ASM International: Almere, The Netherlands, 2004; Volume 9, pp. 994–1020, ISBN 0871707063.
48. Stefanescu, D.M.; Ruxanda, R. Fundamentals of Solidification. In *Metallography and Microstructures Vol 9—ASM Handbook*; Vander Voort, G.F., Ed.; ASM International: Almere, The Netherlands, 2004; pp. 71–92.
49. Ferreira, A.F.; De Castro, J.A.; De Olivé Ferreira, L. Predicting Secondary-Dendrite Arm Spacing of the Al-4.5wt%Cu Alloy during Unidirectional Solidification. *Mater. Res.* **2017**, *20*, 68–75. [CrossRef]
50. Sharma, P. Analysis Anddesign of Cooling Chamber for Gas Atomization Plant. *Int. J. Curr. Res.* **2017**, *9*, 46614–46625.
51. Tourret, D.; Reinhart, G.; Gandin, C.A.; Iles, G.N.; Dahlborg, U.; Calvo-Dahlborg, M.; Bao, C.M. Gas Atomization of Al-Ni Powders: Solidification Modeling and Neutron Diffraction Analysis. *Acta Mater.* **2011**, *59*, 6658–6669. [CrossRef]